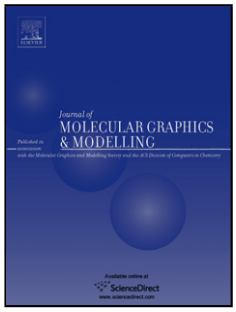

Title: Mechanism and kinetic study of 3-fluoropropene with hydroxyl radical reaction

Author: Yunju Zhang Kai Chao Xiumei Pan Jingping Zhang Zhongmin Su Rongshun Wang

PII: S1093-3263(13)00158-7
DOI: http://dx.doi.org/doi:10.1016/j.jmgm.2013.09.003
Reference: JMG 6334

To appear in: *Journal of Molecular Graphics and Modelling*

Received date: 23-6-2013
Revised date: 4-9-2013
Accepted date: 4-9-2013

Please cite this article as: Y. Zhang, K. Chao, X. Pan, J. Zhang, Z. Su, R. Wang, Mechanism and kinetic study of 3-fluoropropene with hydroxyl radical reaction, *Journal of Molecular Graphics and Modelling* (2013), http://dx.doi.org/10.1016/j.jmgm.2013.09.003

Graphic Abstract

Highlights:

Potential energy surface for the title reaction has been investigated theoretically. Multichannel RRKM theory is employed to calculate the rate constants. The predicted rate constants are in agreement with the available experimental values.

Mechanism and kinetic study of 3-fluoropropene with hydroxyl radical reaction

Yunju Zhang,[1] Kai Chao,[2] Xiumei Pan,[1] Jingping Zhang[1], Zhongmin Su[1] and Rongshun Wang[1!]

[1]*Institute of Functional Material Chemistry, Faculty of Chemistry, Northeast Normal University, Renmin Road 5268. Changchun, Jilin 130024, P. R. China*

[2]Ningxia Entry-Exit Inspection and Quarantine Bureau, Yinchuan, Ningxia 750001, P.R. China

Abstract: Potential energy surface for the reaction of hydroxyl radical (OH) with 3-fluoropropene (CH_2=$CHCH_2F$) has been studied to evaluate the reaction mechanisms, possible products and rate constants. It has been shown that the CH_2=$CHCH_2F$ with OH reaction takes place via a barrierless addition/elimination and hydrogen abstraction mechanism. It is revealed for the first time that the initial step for the barrierless additional process involves a pre-reactive loosely bound complex (CR1) that is 1.60 kcal/mol below the energy of the reactants. Subsequently, the reaction bifurcates into two different pathways to form IM1 ($CH_2CHOHCH_2F$) and IM2 ($CH_2OHCHCH_2F$), which can decompose or isomerize to various products via complicated mechanisms. Variational transition state model and multichannel RRKM theory are employed to calculate the temperature-, pressure-dependent rate constants and branching ratios. At atmospheric pressure with He as bath gas, IM1 formed by collisional stabilization is dominated at T ≤ 600K; whereas the direct hydrogen

[!] Corresponding author. Email address: wangrs@nenu.edu.cn Tel.: 0431-85099511; Fax: 0431-85099511

abstraction leading to CH_2CHCHF and H_2O are the major products at temperatures between 600 and 3000 K, with estimated contribution of 72.9% at 1000 K. Furthermore, the predicted rate constants are in good agreement with the available experimental values.

Key words: CH_2=$CHCH_2F$; OH; transition state; rate constant; RRKM theory

1. Introduction

Due to the adverse environmental impact of chlorofluorocarbons (CFCs) on stratospheric ozone and global warming [1,2], the international community prompted various nations to adopt the Montreal Protocol and its subsequent amendments that phased out the production of CFCs. Saturated hydrofluorocarbons (HFCs) have been used as alternatives to CFCs because the absence of chlorine and bromine atom and thus, should pose no threat to the stratospheric ozone layer [3]. But HFCs still contain C-F bond that could contribute to global warming. As HFCs have at least one C-H bond, they are susceptible to abstract by hydroxyl radical [4], and hence have a shorter lifetime than CFCs. It is well known that C=C bonds are generally more reactive than C-H bonds towards attack by OH radicals. Compared to the corresponding saturated compound, the presence of a C=C bond is expected to lead to increasing reactivity towards OH radicals, decreased atmospheric lifetime, and decreased global warming potentials (GWPs) of HFCs [5]. Therefore, it is necessary to estimate the atmospheric lifetime of such unsaturated HFCs, accurate data for the rate constants and their temperature- and pressure-dependences of the reaction with

OH radical. In this work, we focus on investigating the mechanisms and kinetics of the reaction of 3-fluoropropene with hydroxyl radical.

The 3-fluoropropene molecule has been the subject of several spectroscopic studies for two decades, including infrared, raman, microwave, and NMR spectroscopies [6-9]. Early investigations mostly focused on the conformational isomerism of 3-fluoropropene (CH_2=$CHCH_2F$), which exists as a mixture of cis and gauche rotamers in the gas phase at ambient temperature. Many experimental and theoretical investigations have shown the cis conformer to be the energetically lower lying isomer. However, the measurement of the rate coefficient and kinetic data on the reaction of 3-fluoropropene with hydroxyl radical is both scarce on experimentally and theoretically. Up to date, only Albaladejo et al [10]. studied the absolute rate coefficients for the title reaction at 100-600 Torr pressures and over the temperature range of 228-328 K using the pulsed laser photolysis/laser-induced fluorescence technique. The Arrhenius expression obtained was (6.3! 2.0)! 10^{-12} exp[(285! 94)/T] cm^3 $molecule^{-1}s^{-1}$. The investigation of the mechanism and rate coefficients for the CH_2=$CHCH_2F$ + OH reaction is required to estimate possible products, fate and harmful effects in the atmosphere. In this work, we carried out a detailed theoretical study of the reaction of 3-fluoropropene with OH radicals to gain insight into the reaction mechanism. Multichannel master-equation/RRKM approach and transition state theory have been employed to calculate the rate constants over a wide range of temperatures and pressures.

2. Computational Methods

The geometries of the reactants, products, various intermediates and transition states were fully optimized at the M06-2X/6-311++G(d,p) level [11,12]. It is very important to test the reliability of the method to model the title reaction. Therefore, all the intermediates and transition states are also optimized using the BHandHLYP [13,14] and MP2 [15] methods with the same basis set. It appears that the results are insensitive to the methodology employed in the geometry optimization. Vibrational frequencies calculated at the M06-2X/6-311++G(d,p) level are used to prove the characters of the transition state (number of imaginary frequencies NIMAG=1) and the minimum (NIMAG=0). The intrinsic reaction corrdinate (IRC) method was used to confirm that the transition states connect between designated reactants and products [16]. For the pathways being identified to be the most significant, the coupled cluster CCSD(T)/cc-pVTZ [17] and the multi-coefficient correlation MC-QCISD method [18] with M06-2X/6-311++G(d,p), BHandHLYP/6-311++G(d,p) and MP2/6-311++G(d,p) zero-point energy corrections are calculated. It is known that the CCSD(T) method has a very high accuracy for the small molecule reaction and gives accurate energies for various reactions [19-21]. To gain an insight on multireference character for the stationary points, the T_1-diagnostic is monitored using the CCSD(T)/cc-pVTZ method. A number of studies have shown that the value of T_1 diagnostic up to 0.045 may be acceptable for the open-shell systems [22]. The T_1 values of all species in our system are smaller than 0.045, indicating that multireference character in the CCSD(T) wave functions is not a problem. All the electronic structure calculations in this work were

performed using the GAUSSIAN 09 suit of program packages [23].

The rate constants for the important product channels of the CH_2=$CHCH_2F$ +OH reaction have been calculated using the transition-state theory (TST) and multichannel RRKM theory [24] by the Fortran code. The methodology has been successfully used to deal with the complex reactions [25-29].

3. Results and Discussion

For the present system, there are enantiomorphs. For convenient and clear discussion, we only present moieties of reaction channels that have enantiomorphic varieties and some important enantiomorphous structures. The optimized structures for reactants, products, complexes, intermediates and transition states at three levels of theory are shown in Fig. 1. In order to clarity the reaction mechanism, schematic potential energy profile for the CH_2=$CHCH_2F$ +OH reaction is plotted in Fig. 2. Table 1 summarizes T_1 diagnostic value, relative energies, reaction enthalpies and Gibbs free energy. The moment of inertia, rotational symmetry numbers and harmonic vibrational frequencies of all species involved in this reaction are deposited in Table S1 and S2, respectively. The frequencies of CH_2CHOH, CH_3CHO, CH_2F, CH_2O, CH_3, HOF, H_2O and OH are in agreement with experimental data [30]. Unless otherwise specified, the geometric parameters and energies used in the following discussion are at CCSD(T)/cc-pVTZ//M06-2X/6-31++G(d,p) level with ZPE corrections (without scaled).

3.1 Potential energy surface

Singleton and Cvetanovic proposed that the OH-radical/molecule reactions often

involve complex mechanisms [31]. Similar with other alkenes with OH radicals (e.g., C_2H_4, CH_3CHCH_2, unsaturated alcohol as well as aldehydes) [32-39], the title reaction proceeds via forming of a pre-reactive complex for the initial addition of OH radicals to the unsaturated C=C double bond of CH_2=$CHCH_2F$.

3.1.1 Initial Association

The interaction between the electron deficient O atom of the OH radical and the electron cloud of the double C=C bond in CH_2=$CHCH_2F$ molecule is barrierless with the formation of a pre-reactive van der Waals complex CR1, in which the distances between the oxygen atom of the HO moiety and the two carbon atoms of the C=C double bond of the CH_2CHCH_2F moiety are very long (*i.e.*, 2.892 and 2.580 Å) and the hydrogen bonding between the hydrogen atom of the HO moiety and the F atom of the CH_2CHCH_2F moiety is 2.186 Å. Therefore, CR1 is a loosely bound van der Waals complex. A similar phenomenon was found in the reaction of OH with CF_3CHCH_2 [29], CH_2=$C(CH_3)CH_2OH$ [36] and CH_2=$CHCH_2CH_2OH$ [37]. It should be mentioned that there is no hydrogen bonding in CR1 calculated at the MP2 level, with the hydrogen atom of the OH moiety pointing toward the double bond. The calculated relative energy ΔE of CR1 is 1.60 kcal/mol below the reactants.

After forming the pre-reactive complex CR1, the reaction bifurcates into two different pathways. The energetically most favorable pathway is the addition of OH to the central carbon atom of the C=C double bond to form IM1 ($CH_2CHOHCH_2F$) via the transition state TS1. TS1 shows a conserved character of the C=C double bond and the distance of the C─O bond is 2.110 Å, indicating that TS1 is a reactant-like

transition state structure, which is in accordance with the reaction exothermicity of 28.46 kcal/mol. TS1 lies 0.46 kcal/mol below the energy of the reactants and 1.14 kcal/mol above the energy of CR1. The IRC calculation showed that TS1 goes back to CR1 and goes forward to IM1 ($CH_2CHOHCH_2F$).

As can be seen from Fig. 1, the O atom of the -OH group can also add to the terminal carbon atom of the C=C double bond forming intermediate IM2 ($CH_2OHCHCH_2F$) via transition state TS2. Similar to TS1, distance between the reacting carbon and O atom of OH is as long as 2.125 Å. Therefore, TS2 also shows a reactant-like transition state structure. It lies 0.94 kcal/mol above the energy of the reactants, which is 1.40 kcal/mol higher than that of TS1. The exothermicity of IM2 ($CH_2OHCHCH_2F$) is 25.98 kcal/mol. As shown in Fig. 2 and Table 1, IM1 and IM2 lies 27.50 and 25.01 kcal/mol below the reactants, respectively, and the heat of reaction can provide energy to make IM1 and IM2 activated, which means that once they are formed, the excess energy allows isomerization and decomposition to readily take place. Many production channels of IM1 and IM2 have been found and will be discussed separately in the following part.

3.1.2 The unimolecular reactions of IM1

Starting from IM1, there are many possible reaction pathways. Two types of reactions mechanisms have been found, namely, dissociation mechanism and isomerization/dissociation mechanism.

As seen in Fig. 2, the most feasible decomposition channel of IM1 is the formation of P1 ($CH_2F + CH_2CHOH$) via the C─C bond fission transition state TS3

overcoming a barrier of 30.72 kcal/mol. The breaking C─C bond is 0.675 Å longer than that in the IM1. The second dissociation route is the simple C─H bond cleavage of IM1 via transition state TS4 to form the products P2 (H + CH_2COHCH_2F), in which the breaking C─H bond is elongated from 1.095 to 1.838 Å. The barrier height for TS4 is 34.42 kcal/mol, which is 5.98 kcal/mol higher than TS3. The predicted heat of reaction for the formation of P1 (CH_2F + CH_2CHOH) and P2 (H + CH_2COHCH_2F) are -6.83 and 1.64 kcal/mol, and the overall ΔG for the two channels are -8.88 and 4.46 kcal/mol, respectively. It is conceivable the formation of P2 (H + CH_2COHCH_2F) should be less competitive than that of P1 (CH_2F + CH_2CHOH).

Two isomerization channels from IM1 leading to IM3 (CH_3CHOCH_2F) and IM4 (CH_3COHCH_2F). Then the two isomers can undergo further changes to form the corresponding products. The hydrogen atom of the HO moiety in IM1 can shift to the C atom of the -CH_2 group to give rise to IM3 (CH_3CHOCH_2F) via a four-member-ring transition state TS5. The breaking C─H bond is elongated to 1.264 Å and the forming C-H bond is 1.334 Å. The barrier height for TS5 is 31.79 kcal/mol, which is 2.63 kcal/mol lower than TS4 and 1.07 kcal/mol higher than TS3, and the overall ΔG is 13.52 kcal/mol. IM3 has a relative energy of -19.13 kcal/mol with respect to the initial reactants, which is the most unstable adduct on the OH + CH_2=$CHCH_2F$ potential energy surface. Two separate channels were taken into account for IM3, namely, the C─C bond dissociation to the products P3 (CH_2F + CH_3CHO) via TS6 or P4 (CH_3 + CH_2FCHO) via TS7, which is exothermic by 17.31 and 14.12 kcal/mol, respectively. TS6 and TS7 are 8.11 and 5.67 kcal/mol lower than

reactants and the overall ΔG is 0.31 and 2.81 kcal/mol, and the predicted heat is -9.12 and -6.64 kcal/mol, respectively. Therefore, these two decomposition pathways of IM3 may compete with each other in both kinetically and thermodynamically.

In addition to the above four-center H-shift path, the hydrogen atom of the central carbon atom can also migrate to the $-CH_2$ group of IM1 via TS8 to form isomer IM4 (CH_3COHCH_2F). This is a three-center mechanism in which the breaking C─H bond is elongated to 1.289 Å, and the forming C─H bond is 1.325 Å. The barrier height is 38.45 kcal/mol with respect to IM1, which is 6.66 kcal/mol higher than TS5. It is rationalized that the four-center isomerization involves a lower barrier than the three-center isomerization. IM4, -35.46kcal/mol relative to the initial reactants, can directly decompose to the final product P5 ($H + CH_3COCH_2F$) via the C─H bond cleavage (TS9), needing to overcoming a high barrier height 34.68 kcal/mol. However, TS9 is still lower than the reactants by 0.78 kcal/mol and TS8 by 11.73 kcal/mol, indicating that P5 is easily yielded once IM4 is formed by increasing temperatures.

3.1.3 The unimolecular reactions of IM2

One dissociation and two isomerization/dissociation pathways for the subsequent reactions of IM2 have been obtained. Starting from IM2, the lowest-energy barrier reaction pathway is the production of P6 ($H + CHOHCHCH_2F$) via transition state TS10. This is a simple C─H bond fission process. The breaking C─H bond is elongated to 1.852 Å, which is about 0.757 Å longer than that in IM2. Obviously, TS10 is a later barrier, in accordance with the reaction endothermicity of 1.88

kcal/mol. The barrier of TS10 is 32.21 kcal/mol, which is 3.77 kcal/mol higher than that of IM1→P1 (CH_2F + CH_2CHOH), and the overall ΔG is 15.80 kcal/mol. Therefore, it could be anticipated that the decomposition channel of IM2 should play a less important role in the reaction.

As showed by TS11 in Fig. 1, the hydrogen atom of HO moiety migrating to the central carbon atom to generate intermediate IM5 ($CH_2OCH_2CH_2F$) via a four-member-ring cyclic structure (TS11). The formation of IM5 ($CH_2OCH_2CH_2F$) is the same as that of IM3 (CH_3CHOCH_2F). The breaking O─H bond is elongated to 1.261 Å and the forming C─H bond is 1.336 Å. Meanwhile, the C─O bond is elongated by 0.014 Å. The barrier height for TS11 is about 31.44 kcal/mol relative to IM2, which is above the initial reactants by 6.43 kcal/mol. IM5, -22.70 kcal/mol with respect to the initial reactants, either breaks the C─C bond to give rise to P7 (CH_2O + CH_2CH_2F) via TS12 or ruptures C─H bond to produce P8 (H + CH_2FCH_2CHO) via TS13, respectively. The corresponding barrier heights are 16.97 and 23.47 kcal/mol respectively. The former is expected to be more easily to take place than the latter one. TS12 is lower than reactants by 5.73 kcal/mol and TS11 by 12.16 kcal/mol. These results indicate that the formation of P7 (CH_2O + CH_2CH_2F) channel by C─C cleavage is more favorable than the formation of P8 (H + CH_2FCH_2CHO).

In addition, IM2 can also isomerize to IM6 ($CHOHCH_2CH_2F$) via 1,2-hydrogen migration transition state TS14 with a barrier of 40.89 kcal/mol. The dissociation pathways of IM6 are similar to the decomposition channels of IM5. Two product channels are found for IM6, namely, the C─C bond cleavage to form P1 (CH_2F +

CH_2CHOH) via TS15, and the hydrogen atom loss to form P8 (H + CH_2FCH_2CHO) via TS16. The barrier heights are 31.22 kcal/mol and 34.88 kcal/mol, respectively. The energy of TS15 is lower than TS14 by 14.60 kcal/mol and TS3 by 1.94 kcal/mol, respectively. Therefore, direct dissociation of IM1 leading to P1 (CH_2F + CH_2CHOH) has priority over the IM2→TS14→IM6→TS15→P1 (CH_2F + CH_2CHOH).

Besides these investigations, we also studied the intramolecular elimination of the H atom and OH radical group to form H_2O. Moreover, three H_2O-elimination paths have been found, starting from IM2, IM1 and IM6, leading to h-P1 (H_2O + CH_2CHCHF), h-P2 (H_2O + CH_2CCH_2F) and h-P3 (H_2O + cis-$CHCHCH_2F$), respectively. The corresponding barrier heights are 52.87 kcal/mol (TS17), 74.28 kcal/mol (TS18) and 69.08 kcal/mol (TS19), respectively. Evidently, water molecule production in these mechanisms could be negligible. Note that the geometries of TS17 are not found at the BHandHLYP/6-311++G(d,p) level of theory. Water formation via a direct hydrogen abstraction mechanism is more favored as detailed below.

3.1.4 Abstraction Mechanism

In the C_s symmetry CH_2=$CHCH_2F$ molecule, four possible abstraction channels have been found and Fig. 2 shown the corresponding energies profiles. There are four different chemical environments of the H atom. The OH radical can abstract the H atoms in -CH_2F group to form h-P1 (H_2O + CH_2CHCHF) via transition state h-TS1. In h-TS1, The lengths of the breaking C─H and the newly formed O─H bond are 1.161 and 1.458 is Å, respectively, which are 6.1% and 52.0% longer than the equilibrium bond lengths of C─H in CH_2=$CHCH_2F$ and O─H in H_2O. The elongation

of the forming bond is greater than that of the breaking bond, therefore, h-TS1 is reactant-like transition state, and the channels proceed via an early barrier. The relative energy of h-TS1 is 1.14 kcal/mol. It is noted that h-P1 (H_2O + CH_2CHCHF) is the most stable product on the PES. This is because that CH_2CHCHF has a C=C=C double-double-bond-like structure, and all atoms are in the plane CCCF. Another channel corresponds to the H abstraction by OH radical from the central C atom of CH_2=$CHCH_2F$, leading to h-P2 (H_2O + CH_2CCH_2F) via the transition state h-TS2. The barrier height is 4.76 kcal/mol, which is 3.62 kcal/mol higher than that of h-TS1. In h-TS2, the forming O─H bond is 1.310 Å, which is 0.351 Å longer than the equilibrium distance in the H_2O molecule, while the breaking C─H bond is elongated by 0.115 Å. The last possible channel involved is that the OH radical abstracts the hydrogen atom in the =CH_2 group to yield h-P3 (H_2O + cis-$CHCHCH_2F$) and h-P4 (H_2O + trans-$CHCHCH_2F$) via h-TS3 and h-TS4, respectively. The corresponding barrier heights are 5.46 and 6.04 kcal/mol, respectively. In addition, the F atom in CH_2=$CHCH_2F$ can also be abstracted by OH radicals via f-TS1. The barrier height, 61.96 kcal/mol, is rather high. Furthermore, the product f-P1 (HOF + CH_2CHCH_2) lies at the point of 49.85 kcal/mol above the reactants. Due to higher barrier height and unstable product, the pathway of fluorine abstraction is not important to the title reaction. In summary, the formation of h-P1 (H_2O + CH_2CHCHF) is more thermodynamically feasible in view of the exothermicities of four abstraction routes (e.g., 30.92, 6.33, 3.26 and 3.78 kcal/mol for h-P1, h-P2, h-P3 and h-P4, respectively).

3.2 Rate constants calculation

Another major goal of this study is to predict the reaction rate constants and compared with experimental data. According to the calculated barrier heights, a simplified version of the mechanism which may cover all the important reaction routes for the OH + CH_2! $CHCH_2F$ reaction is shown in Scheme 1-3. The kinetic calculation for various product channels is calculated using transition state theory and mulitchannel RRKM theory on the basis of ab initio energetics, frequencies and moments of inertia of various relevant species. For the two essentially barrierless pathways, namely, OH + CH_2=$CHCH_2F$! CR1 ! IM1 or IM2, a variational treatment is required for such processes. The energies along the reaction coordinate (R_{CO}) are calculated at CCSD(T) and M06-2X/6-311++G(d,p) level of theory (Fig. 3). The variation of the dividing surface of the transition state was carried out in the range of R_{CO}=2.0–3.4 Å, with the step size of 0.1 Å. The energy and the rotational constant for each point were obtained by interpolation.

As we all know, it is hardest to evaluate the vibrational partition function of the transition state. The flexible transition state theory which developed by Klippenstein et al. could be employed but required a full-dimensional potential energy surface [40-43]. Alternatively, the vibrational frequencies for each optimized structure along the reaction coordinates could be calculated. However, it is hard to extrapolate these frequencies in the variational treatment because it is difficult to identify the individual vibrational mode correctly. For simplicity, the vibrational frequencies for the variational transition state are considered to be those of the reactants (OH and

CH_2CHCH_2F), together with four "intermolecular frequencies", after excluding the C! O stretch vibration along the reaction coordinate. Among the four "disappearing" frequencies, the O-H rotation around the C-O coordinate was considered to be the onedimensional free internal rotor, with the reduced moment of inertia of 9.74 amu. The other three disappearing vibrational frequencies were calculated from the corresponding normal modes of IM1 or IM2 using the following exponential expression:

$$v(R)=v(R_e)!\ e^{-!\ (R-Re)}$$

where R_e is the equilibrium C! O bond length in IM1 or IM2 and the parameter ! is a fitting parameter. This approximation is reasonable because the variational transition states along the reaction coordinates are very loose, that is, reactant-like. Although this methodology is not *a priori*, it is the simplest procedure to simulate the dependence of the rate coefficients on both temperatures and pressures.

The reaction paths including in Scheme 1-3 are considered in the following calculation:

SCHEME 1

$$CH_2CHCH_2F + OH \underset{1}{\overset{a}{\rightleftharpoons}} IM1 \xrightarrow{2} P1: (CH_2F + CH_2CHOH)$$

SCHEME 2

$$CH_2CHCH_2F + OH \underset{1}{\overset{a}{\rightleftharpoons}} IM2 \xrightarrow{2} P6: (H + CHOHCHCH_2F)$$

SCHEME 3

$$CH_2CHCH_2F + OH \longrightarrow h\text{-}P1$$
$$\longrightarrow h\text{-}P2$$
$$\longrightarrow h\text{-}P3$$
$$\longrightarrow h\text{-}P4$$

$$IMj^* \xrightarrow{!} IMj$$

where ! * ! represents the vibrational excitation of the intermediate (IMj). Steady-state assumption for energized intermediate (IMj*) leads to the following expressions:

For SCHEME 1:

$$k_{IM1}(T,P) ! \frac{! _a}{h} \frac{Q_t^! Q_r^!}{Q_{CH_2 ! CHCH_2F} Q_{OH}} e^{! E_a / RT} ! \int_{!0}^{!} \frac{!}{k_1(E) ! \ k_2(E) ! \ !} N_a(E^!) e^{! E^! / RT} dE^! \quad (1)$$

$$k_{P1}(T,P) ! \frac{! _a}{h} \frac{Q_t^! Q_r^!}{Q_{CH_2 ! CHCH_2F} Q_{OH}} e^{! E_a / RT} ! \int_{!0}^{!} \frac{k_2(E)}{k_1(E) ! \ k_2(E) ! \ !} N_a(E^!) e^{! E^! / RT} dE^! \quad (2)$$

For SCHEME 2:

$$k_{IM2}(T,P) ! \frac{! _a}{h} \frac{Q_t^! Q_r^!}{Q_{CH_2 ! CHCH_2F} Q_{OH}} e^{! E_a / RT} ! \int_{!0}^{!} \frac{!}{k_1(E) ! \ k_2(E) ! \ !} N_a(E^!) e^{! E^! / RT} dE^! \quad (3)$$

$$k_{P6}(T,P) ! \frac{! _a}{h} \frac{Q_t^! Q_r^!}{Q_{CH_2 ! CHCH_2F} Q_{OH}} e^{! E_a / RT} ! \int_{!0}^{!} \frac{k_2(E)}{k_1(E) ! \ k_2(E) ! \ !} N_a(E^!) e^{! E^! / RT} dE^! \quad (4)$$

The microcanonical rate constant is calculated using the RRKM theory as follows:

$$k_i(E) ! \ ! \ _i C_i N_i(E_i^!) / h ! \ _j(E_j) \quad (10)$$

In the above equations, $! \ _a$ is the statistical factor for the reaction path a, and $! \ _i$ is the statistical factor (degeneracy) for the *i*th reaction path; E_a is the energy barrier for the

reaction step a. Q_{OH} and $Q_{CH_2!\,CHCH_2F}$ are the total partition function of OH and CH_2=$CHCH_2F$, respectively; $Q_t^!$ and $Q_r^!$ are the translational and rotational partition functions of entrance transition state, respectively; $N_a(E^!)$ is the number of state for the association transition state with excess energy $E^!$ above the association barrier. $k_i(E)$ is the energy-specific rate constant for the *i*th channel, and C_i is the ratio of the overall rotational partition function of the TS_i and IM_j; $N_i(E_i^!)$ is the number of states at the energy above the barrier height for transition state *i*; $!_j(E_j)$ is the density of states at energy E_j of the intermediate. The density of states and the number of states are calculated using the extended Beyer-Swinehart algorithm [44,45]. The collision deactivation rate $\omega = \beta_c Z_{LJ}[M]$; in here, β_c is the collision efficiency calculated using Troe's weak collision approximation [46] with the energy transfer parameter -<ΔE>, The simple expression for collisional energy transfer (-<ΔE>) [47, 48] is

$$\frac{!_c}{1!\ !_c^{1/2}}!\ \frac{!\ !!\ E!}{F_E kT}$$

This expression holds nearly exactly at the weak collision limit -<ΔE> ! ! $F_E kT$ for all collision models [47,48]. The factor F_E is set to 1.0 empirically. The average energy transfer per collision, *i.e.*, -! ΔE! , is unknown and cannot be calculated quantitatively. In consideration of the experimental rate constants, it is found that the values around 100 cm^{-1} for -! ΔE! should be reasonable to calculate the rate constants. Z_{LJ} is the Lennard-Jones collision frequency. The collision efficiency is estimated using the Lennard-Jones potential ($V(r) = 4\varepsilon[(\sigma/r)^{12} - (\sigma/r)^6]$) by fitting the interaction energies calculated at the M06-2X/6-311++G(d,p) level for IM1…He and IM2…He. It is estimated that (ε = 63.14 K, σ =2.72 Å) for IM1…He and (ε =196.37 K, σ = 2.54

Å) for IM2…He, and [M] is the concentration of the bath gas M (He). The weak collision approximation is used for the intermediate.

The rate coefficients for the direct hydrogen abstraction routes can be readily obtained using the conventional transition-state theory, viz.:

$$k_{abs}(T) = \kappa_1 \frac{k_B T}{h} \frac{Q_{TS}^{!}}{Q_{CH_2=CHCH_2F} Q_{OH}} e^{-E_1/(RT)}$$

where κ_1 is the tunneling factor, k_B and h are Boltzmann and Planck constants, respectively. $Q_{TS}^{!}$, $Q_{CH_2=CHCH_2F}$ and Q_{OH} are the h-TS1 (h-TS2, h-TS3 or h-TS4), CH_2=$CHCH_2F$ and OH partition functions, respectively. E_1 is the energy barrier of h-TS1 (h-TS2, h-TS3 or h-TS4). The unsymmetrical Eckart potential model is employed to estimate κ_1 [49,50].

The temperature dependence of the total and individual rate constants is shown in Fig. 4 at the pressure of 100 Torr of He. The available experimental data are also included for comparison. The calculated total rate constants (k_{tot}) in He are in good agreement with the relevant experiment data given by Albaladejo.[10] (k_{tot}=1.66$\times 10^{-11}$ cm^3 $molecule^{-1}s^{-1}$ vs. (1.62$\pm$0.26)$\times 10^{-11}$ at 298 K). The entrance additional channel rate constant (central-C (k_{IM1}) and terminal-C (k_{IM2})) show negative temperature dependence at the whole temperature range (at 200─3000 K). Especially when T ≥ 600K, these rate constants sharply decrease, which can be explained that the stabilization of IM1 and IM2 become unimportant due to the rapid decomposition rate of IM1 and IM2 and the hydrogen abstraction channels become more important at high temperatures. The hydrogen abstraction rate constants for $k_{h\text{-}P1}$ (-CH_2F group), $k_{h\text{-}P2}$ (-CH group) and $k_{h\text{-}P3}$ (-CH_2 group) are positive temperature dependence. At

200─500 K, k_{IM1} approaches to k_{tot}, meanwhile $k_{h\text{-}P1}$ for direct hydrogen abstraction is close to k_{tot} at 700─3000 K, moreover at T=600 K, the rate constants for $k_{h\text{-}P1}$ and k_{IM1} are almost identical. Thus, the total rate constant is decreasing with the temperature increasing (at 200─600 K) and increasing with the temperature increasing (at 600─3000K), indicating strong temperature dependence.

We also select the atmospheric pressure (P=760 Torr) and perform the temperature dependence of the rate constants for the title reaction (Fig. 5). As can be seen from Fig. 5 that similar changes occur at 760 Torr He. At T=298 K and P=760 Torr, the total rate constant is 2.28! 10^{-11} cm^3 $molecule^{-1}s^{-1}$. For practical use, the predicted total rate constants (in units of cm^3 $molecule^{-1}s^{-1}$) at 760 Torr He in 200-3000 K can be represented as below:

k_{tot}=2.10! 10^{-7} $T^{1.60}$ exp(-3.48/T) (200 ! T! 700)

k_{tot}=8.28! 10^{-11} $T^{0.38}$ exp(-6303.17/T) (700 ! T! 3000)

Total rate constants calculated at several pressures with available experimental data are given in Fig. 6. The total rate constant shows positive pressure dependence at low and moderate temperatures and shows pressure independence at higher temperatures. The high-pressure limit rate constants decrease first as the temperatures increase at T < 450 K, and then increase monotonously. This marked change is due to a change of the dominant reaction pathway, from the additional channels at low and moderate temperatures to the other including hydrogen abstraction channels at higher temperatures. This typical phenomenon is also observed in the analogical reactions of OH with C_2H_4 [31].

Product branching ratios as a function of temperature are shown in Figs. 7(a), 7(b) and 7(c) for the atmospheric pressure, high-pressure limit and collisionless limit of He, respectively. Under 760 Torr He, the yield of stabilized IM1 drops with increasing temperatures, from 90.4% at 200 K down to 65.7% at 500 K, and 3.3% at 1000K, whereas the yield of the -CH_2F group-H abstraction channel product ($CH_2CHCHF + H_2O$) sharply rises with increasing temperatures first (at 273-1000 K), from 1% at 273 K up to maximal point of 72.9% at 1000K, but drops with increasing temperatures (T≥1200 K), from 69.6% at 1200 K down to 46.8% at 3000 K. While from 600 to 3000K the branching ratios of the h-P2 and h-P3 rise with increasing temperatures. As for IM2, the branching ratios increase steeply first, and then decrease slowly. The branching ratios of other products are too small to compete throughout the entire temperature range investigated. So they are not explained here. Whereas the results of high-pressure limit and collisionless limit have difference, the yield of product ($H_2O + CH_2CHCHF$) has a dominant attribution to the reaction at the whole temperature range at low pressures. While at high-pressure limit, the major products are IM1 over the temperature range (200-500 K); the channel leading to ($H_2O + CH_2CHCHF$) becomes dominant above 600 K and IM2, h-P2 and h-P3 become important at higher temperatures. It is indicated that temperature and pressure will affect the yield of products.

Figs. 8 and 9 present the predicted total rate constant and branching ratio over a wide pressure range 10^{-14}-10^{14} Torr in the bath gas of He at temperatures 298, 500 and 1000 K, respectively. It is obvious that Fig. 8 shows typical falloff behavior for the

complex-forming reactions. The falloff range shifts to high pressure with increasing temperature. The falloff region of the total rate constants ranges from 10^{-2} to 10^{3} Torr at 298 K and 10^{0} to 10^{4} Torr at 500 K, as well as 10^{5} to 10^{8} Torr at 1000 K. Meanwhile, it can be seen from Fig. 9, at 298 K, the major products are h-P1 (H_2O + CH_2CHCHF) at $P \leq 10^{-1}$ Torr. The stabilization of the IM1 becomes dominant and a significant fraction of the total reaction leads to IM2 at higher pressure range. Whereas the results at 500 and 1000 K have difference, IM2 becomes more and more important with increasing temperatures, even at T=1000K, the branching ratios of IM2 are higher than that of IM1 at the pressure range(10^{6}-10^{14} Torr).

An unsymmetrical Eckart potential was used to calculate the tunneling factor κ. For the addition/elimination mechanism, the κ was always in the range 1.2-1.0; while 2.3-1.0 for the main direct hydrogen abstraction step (-CH_2F group-H abstraction) at the whole temperature region (200-3000K) as bath gas of He. For the -CH_2 group-H and -CH group-H abstraction channels, the κ is relatively large at the low temperatures. For example, the values of κ at 200, 298 and 500 K are 21.6, 3.7 and 1.6 for the -CH group-H abstraction pathway, respectively. However, this significant tunneling effect cannot influence our kinetic calculations significantly. For example, at 200K, even if the tunneling correction is included, the dominant channel is still the addition with a rate of 4.05×10^{-11} cm^3 $molecule^{-1}s^{-1}$ because this value is a few orders of magnitude higher than that for the -CH group-H and -CH_2 group-H abstraction pathway (about 7.05×10^{-17} cm^3 $molecule^{-1}s^{-1}$, 1.47×10^{-16} cm^3 $molecule^{-1}s^{-1}$ and1.36×10^{-17} cm^3 $molecule^{-1}s^{-1}$, respectively). From 1000 to 3000 K, κ is in the range

1.1-1.0. These results indicated that the tunneling effect is not significant at higher temperatures.

As indicated in the introduction, little experimental or theoretical work has been done on this reaction; therefore, a quantitative analysis of the error is necessary. The most important point for accuracy is the reaction threshold, e.g., M06-2X and CCSD(T)/cc-pVTZ calculations. Analysis show that the M06-2X and CCSD(T)/cc-pVTZ calculations would be appropriate for this system, because (i) the M06-2X frequencies are believed to reliable; (ii) the overall rate constant is determined mainly by the barrier height, especially the entrance reaction barrier for addition step. The relative energies calculated with CCSD(T)/cc-pVTZ level of theory have at least a possible error bar of ca. 0.5 kcal/mol. To assess the important changes in reaction threshold, we calculated rate constants with the barrier shifted up or down 0.5 kcal/mol. The results imply that shifting the barrier down or up by 0.5 kcal/mol cause the rate constant to increase or decrease accordingly within a factor. By calculating and analyzing, the rate constant (k_{IM1} and k_{IM2}) is most sensitive to the entrance barrier at low temperatures (T＜500 K). When the assumed reaction barrier is increased or decreased by 0.5 kcal/mol, the reaction rate constant shows a corresponding variation of about a factor of 2 at 500 K, whereas the influence of rate constant is insignificant at higher temperatures. For example at 2000 K, the rate constant will increase or drop about a factor of 1. The branching ratio of IM1 and IM2 has a minor change over the whole temperature range. These are not surprising because the threshold reaction has a barrier (1.14 and 2.54 kcal/mol for IM1 and IM2)

climbed that is affected by low or high temperature.

4. Conclusions

In the present study, the detailed mechanism of the CH_2=$CHCH_2F$ + OH has been investigated at the CCSD(T)/cc-pVTZ//M06-2X/6-311++G(d,p) level. H (or F)-abstraction and the addition/elimination mechanisms are revealed. The initial step for the OH radical attacking on the C=C bond in CH_2=$CHCH_2F$ involves a pre-reactive loosely bound complex with no barrier in the entrance channel, lying 1.60 kcal/mol below the energy of the reactants. Subsequently, the reaction bifurcates into different pathways, the most feasible pathway is the addition of hydroxyl radicals to the central carbon atom of the C=C double bond. The corresponding transition-state lies 0.46 kcal/mol below the reactants. The OH addition to the terminal carbon atom of the C=C double bond involves a higher barrier, namely, 0.94 kcal/mol above the energy of the reactants. However, the H-abstraction (-CH_2F group) is the lowest-energy barrier pathway in the direct abstraction reactions.

The rate calculations, to quantificationally predict the major products, have been carried out by using variational transition state theory and the multichannels RRKM theory. It is predicted that at lower temperatures, the stabilization of the adduct IM1 ($CH_2CHOHCH_2F$) is dominate for the reaction; the total rate constant shows weak temperature dependence. At higher temperatures the production of CH_2CHCHF via hydrogen abstractions becomes dominant; the total rate constant shows positive temperature dependence. Moreover, the title reaction exhibits positive pressure dependence at low and moderate temperature. The total rate constant exhibits the

typical falloff behavior for the complex-forming reactions over a wide range of pressures. The present work will provide useful information for understanding the process of OH radical with other halogen substituted unsaturated hydrocarbons.

Reference

1. M.J. Molina, F.S. Rowland, Stratospheric sink for chlorofluoromethanes: Chlorine-atom catalyzed destruction of ozone. Nature. 249 (1974) 810-812

2. J.D. Farman, B.G. Gardiner, J.D. Shanklin, Large losses of total ozone in Antarctica reveal seasonal CIO,/NO, interaction. Nature. 315 (1985) 207-210

3. T.J. Wallington, W.F. Schneider, D.R. Worsnop, O.J. Nielsen, J. Sehested, W. DeBruyn, J.A. Shorter, Environmental Impact of CFC Replacements-HFCs and HCFCs. Environ. Sci. Technol. 28 (1994) 320A-326A

4. R. Atkinson, In Air Pollution, the Automobile, and Public Health; A.I. Watson, R.R. Bates, D. Kennedy, Eds, National Academic Press: Washington, DC, 1988; pp 99-132

5. B.J. Finlayson-Pitts, J.N. Pitts Jr, Chemistry of the Upper and Lower Atmosphere, Academic Press, London, 2000

6. B. Galabov, J.P. Kenny, H.F. Schaefer III, Conformational Stability of 3-Fluoropropene: A Challenging Problem for Both Theory and Experiment. J. Phys. Chem. A 106 (2002) 3625-3628

7. J.R. Durig, T.J. Geyer, T.S. Little, D.T. Durig, Vibrational Assignment and Conformational Equilibrium for 3-Fluoropropene Based on *Ab Initio* Calculations and High Resolution Far Infrared Spectroscopy. J. Mol. Struct. 172 (1988)165

8. J. Nieminen, J. Murto, M. Rasanen, Matrix isolation infrared and ab initio studies on conformers of 3-fluoropropene . Spectrochim. Acta. 47A (1991) 1495

9. M.O. Bulanin, Spectroscopy of molecules in liquid noble gases. J. Mol. Struct. 347 (1995) 73-82

10. J. Albaladejo, B. Ballesteros, E. Jiménez, Y. Díaz de Mera, E. Martínez, Gas-phase OH radical-initiated oxidation of the 3-halopropenes studied by PLP-LIF in the temperature range 228-388 K. Atmos. Environ. 37 (2003) 2919-2926

11. Y. Zhao, D.G. Truhlar, The M06 suite of density functionals for main group thermochemistry, thermochemical kinetics, noncovalent interactions, excited states, and transition elements: two new functionals and systematic testing of four M06-class functionals and 12 other functionals. Theor. Chem. Account. 120 (2008) 215-241

12. Y Zhao, Truhlar DG (2008) Density Functionals with Broad Applicability in Chemistry. Acc. Chem. Res. 41:157-167

13. A.D. Becke, A new mixing of Hartree–Fock and local density□functional theories. J. Chem. Phys. 98 (1993)1372-1377

14. C. Lee, W. Yang, R.G. Par, Development of the Colle-Salvetti Correlation-Energy Formula into a Functional of the Electron Density. Phys. Rev. B. 37 (1988)785-789

15. C. Møller, M.S. Plesset, Note on an Approximation Treatment for Many-Electron Systems. Phys. Rev. 46 (1934) 618

16. C. Gonzalez, H.B. Schlegel, An improved algorithm for reaction path following. J Chem Phys 90 (1989) 2154-2161; Reaction path following in mass-weighted internal coordinates. J. Phys .Chem. 94 (1990) 5523-5527

17. K. Raghavachari, G.W. Trucks, J.A. Pople, M. Head-Gordon, A Fifth-Order Perturbation Comparison of Electron Correlation Theories. Chem. Phys. Lett. 157 (1989) 479-483

18. P.L. Fast, D.G. Truhlar MC-QCISD: Multi-Coefficient Correlation Method Based on Quadratic Configuration Interaction with Single and Double Excitations. J. Phys. Chem. A. 104 (2000) 6111

19. Z.F. Xu, K. Xu, M.C. Lin, Ab Initio Kinetics for Decomposi- tion/Isomerization Reactions of C_2H_5O Radicals. Chem. Phys. Chem. 10 (2009) 972-982

20. H. Hou, B.S. Wang, Mechanistic and Kinetic Study of the O + CH_2OH Reaction. J. Phys. Chem. A. 109 (2005) 4796-4803

21. H. Hou, L.Z. Deng, J.C. Li, B.S. Wang, A Systematic Computational Study of the Reactions of HO_2 with RO_2: The HO_2 + CH_2ClO_2, $CHCl_2O_2$, and CCl_3O_2 Reactions. J. Phys. Chem. A. 109 (2005) 9299-9309

22. T.J. Lee, P.R. Taylor, A diagnostic for determining the quality of single reference electron correlation methods. Int. J. Quantum. Chem. S23 (1989) 199-207

23. M.J. Frisch, G.W. Trucks, H.B. Schlegel, G.E. Scuseria, M.A. Robb, J.R. Cheeseman, G. Scalmani, V. Barone, B. Mennucci, G.A. Petersson, H. Nakatsuji, M. Caricato, X. Li, H.P. Hratchian, A.F. Izmaylov, J. Bloino, G. Zheng, J.L. Sonnenberg, M. Hada, M. Ehara, K. Toyota, R. Fukuda, J. Hasegawa, M. Ishida, T. Nakajima, Y. Honda, O. Kitao, H. Nakai, T. Vreven, J.A. Montgomery, Jr, J.E. Peralta, F. Ogliaro, M. Bearpark, J.J. Heyd, E. Brothers, K.N. Kudin, V.N. Staroverov, R. Kobayashi, J. Normand, K. Raghavachari, A. Rendell, J.C. Burant, S.S. Iyengar, J. Tomasi, M. Cossi,

N. Rega, J.M. Millam, M. Klene, J.E. Knox, J.B. Cross, V. Bakken, C. Adamo, J. Jaramillo, R. Gomperts, R.E. Stratmann, O. Yazyev, A.J. Austin, R. Cammi, C. Pomelli, J.W. Ochterski, R.L. Martin, K. Morokuma, V.G. Zakrzewski, G.A. Voth, P. Salvador, J.J. Dannenberg, S. Dapprich, A.D. Daniels, O. Farkas, J.B. Foresman, J.V. Ortiz, J. Cioslowski, D.J. Fox, *Gaussian*, Inc, Wallingford CT, 2009.

24. K.A. Holbrook, M.J. Pilling, S.H. Robertson, Unimolecular Reactions; J. Wiley: Chichester, UK, 1996

25. H. Hou, B.S. Wang, Y.S. Gu, Ab Initio Mechanism and Multichannel RRKM−TST Rate Constant for the Reaction of Cl(^{2}P) with CH_2CO (Ketene). J. Phys. Chem. A. 104 (2000) 320

26. Y.J. Zhang, J.Y. Sun, K. Chao, H. Sun, F. Wang, S.W. Tang, X.M. Pan, J.P. Zhang, R.S. Wang. Mechanistic and kinetic study the reaction of O(^{3}P) + CH_3CFCH_2. Theor. Chem. Acc. 131 (2012) 1100-1113.

27. J.Y. Sun, R.S. Wang, B.S. Wang. Theoretical study on the gas phase reaction of acrylonitrile with a hydroxyl radical. Phys. Chem. Chem. Phys. 13 (2011) 16585-16595.

28. H. Hou, B.S. Wang, Ab initio study of the reaction of propionyl (C_2H_5CO) radical with oxygen (O_2). J. Chem. Phys. 127 (2007) 054306-054314

29. Y.J. Zhang, J.Y. Sun, K. Chao, H. Sun, F. Wang, S.W. Tang, X.M. Pan, J.P. Zhang, R.S. Wang, Mechanistic and Kinetic Study of $CF_3CH=CH_2$ + OH Reaction. J. Phys. Chem. A. 116 (2012) 3172-3181

30. NIST Computational Chemistry Comparison and Benchmark Database.

http://srdata.nist.gov/cccbdb/

31. D.L. Singleton, R.J. Cvetanovic, A Two Transition State Model for Radical-Molecule Reactions: A Case Study of the Addition of OH to C_2H_4. J. Phys. Chem. A. 109 (2005) 6031-6044

32. C. Sosa, H.B. Schlegel, An ab initio study of the reaction pathways for OH + C_2H_4 → $HOCH_2CH_2$ → products. J. Am. Chem. Soc. 109 (1987) 4193-4198

33. J.P. Senosiain, S.J. Klippenstein, J. A. Miller, Reaction of ethylene with hydroxyl radicals: a theoretical study. J. Phys. Chem. A. 110 (2006) 6960-6970

34. R.S. Zhu, J. Park, M.C, Lin, Ab initio Kinetic Study of the Low Energy Paths of the HO + C_2H_4 Reaction. Chem. Phys. Lett. 408 (2005) 25-30

35. C.W. Zhou, Z.R. Li, X.Y. Li, Kinetics and Mechanism for Formation of Enols in Reaction of Hydroxide Radical with Propone. J. Phys. Chem. A. 113 (2009) 2372

36. W.C. Zhang, B.N. Du, C.J. Feng, Theoretical investigation on mechanism for OH-initiated oxidation of $CH_2=C(CH_3)CH_2OH$. Theor. Chem. Acc. 125 (2010) 45-55

37. B.N. Du, C.J. Feng, W.C. Zhang, L.L. Wu, Theoretical study on the mechanism for the reaction of OH with $CH_2=CHCH_2CH_2OH$. Chem. Phys. 367 (2010) 52-61

38. S. Olivella, A. Solé, Mechanisms for the Reactions of Hydroxyl Radicals with Acrolein: A Theoretical Study. J. Chem. Theory. Comput. 4 (2008) 941-950

39. S. Scheiner, T. Kar, Analysis of the Reactivities of Protein C−H Bonds to H Atom Abstraction by OH Radical. J. Am. Chem. Soc. 132 (2010) 16450

40. S.J. Klippenstein, Implementation of RRKM theory for highly flexible transition states with a bond length as the reaction coordinate. Chem. Phys. Lett. 170 (1990)

71-77

41. D.M. Wardlaw, R.A. Marcus, On the Statistical Theory of Unimolecular Processes. Adv. Chem. Phys. 70 (1988) 231

42. S. Robertson, A.F. Wagner, D.M. Wardlaw, Flexible Transition State Theory for a Variable Reaction Coordinate: Analytical Expressions and an Application. J. Phys. Chem. A. 106 (2002) 2598-2613

43. S. Robertson, A.F. Wagner, D.M. Wardlaw, Flexible transition state theory for a variable reaction coordinate: Derivation of canonical and microcanonical forms. J. Chem. Phys. 113 (2000) 2648-2661.

44. S.E. Stein, B.S. Rabinovitch, Accurate evaluation of internal energy level sums and densities including anharmonic oscillators and hindered rotors*. J. Chem. Phys. 58 (1973) 2438-2445.

45. D.C. Astholz, J. Troe, W. Wieters, Unimolecular processes in vibrationally highly excited cycloheptatrienes. I. Thermal isomerization in shock waves. J. Chem. Phys. 70 (1979) 5107-5116.

46. G. Klopman, C.M. Joiner, New Evidence in the Mechanism of Ozonolysis of Olefins. J. Am. Chem. Soc. 97 (1975) 5287-5288.

47. J. Troe, Theory of thermal unimolecular reactions at low pressures. I. Solutions of the master equation. J. Chem. Phys. 66 (1977) 4745-4757.

48. J. Troe, Predictive possibilities of unimolecular rate theory. J. Phys. Chem. 83 (1979) 114-126.

49. H.S. Johnston, J. Heicklen, Tunnelling Corrections for Unsymmetrical Eckart

Potential Energy Barriers. J. Phys. Chem. 66 (1962) 532-533

50. C. Eckart, The penetration of a potential barrier by electrons. Phys. Rev. 35 (1930) 1303-1309

Figure caption

Fig. 1 Optimized geometries (length in Å) of the species of the CH_2=$CHCH_2F$ + OH reaction. The first, second and third entries correspond to the BHandHLYP, M06-2X and MP2 values, respectively. The values in italics are experimental data from ref 30.

Fig. 2 The profile of potential energy surface for the CH_2=$CHCH_2F$ + OH reaction. The relative energies are calculated at the CCSD(T)/cc-pVTZ//M06-2X/6-311++G(d,p)+ ZPE level of theory.

Fig. 3 The calculated minimum energy path along the reaction coordinates (R_{CO}) for the addition of OH to the carbon atoms of CH_2=$CHCH_2F$ at the CCSD(T)/cc-pVTZ and M06-2X/6-311++G(d,p) levels.

Fig. 4 Temperature dependence of the total and individual rate constants at 100 Torr of He. The experimental data are included from ref 10.

Fig. 5 Temperature dependence of the total and individual rate constants at 760 Torr of He.

Fig. 6 Total rate constants calculated at several pressures in bath gas of He.

Fig. 7 Branching ratios for the CH_2=$CHCH_2F$ + OH reaction in the temperature range 200-3000 K at (a) atmospheric pressure, (b) high-pressure limit and (c) collisionless limit of He.

Fig. 8 Pressure dependence of the total rate constants for the CH_2=$CHCH_2F$ + OH reaction at 298, 500 and 1000 K.

Fig. 9 Branching ratios of products for the CH_2=$CHCH_2F$ + OH reaction at 298, 500 and 1000 K.

Table caption

Table 1 Relative Energies(! *E*), T_1 diagnostic values, Reaction Enthalpies(! *H*) and Gibbs Free Energy(! *G*) for various species in the OH + CH_2=$CHCH_2F$ reaction

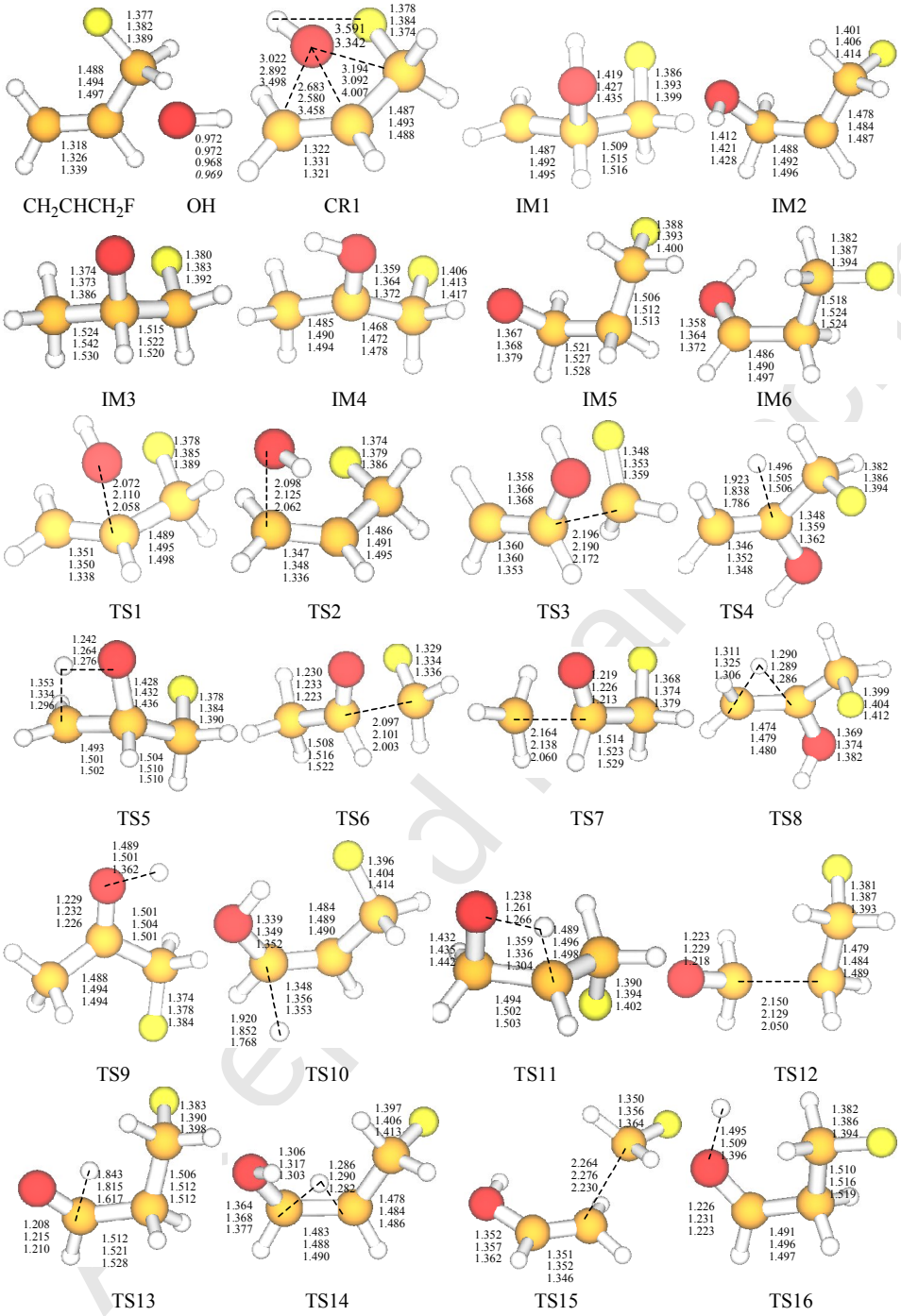

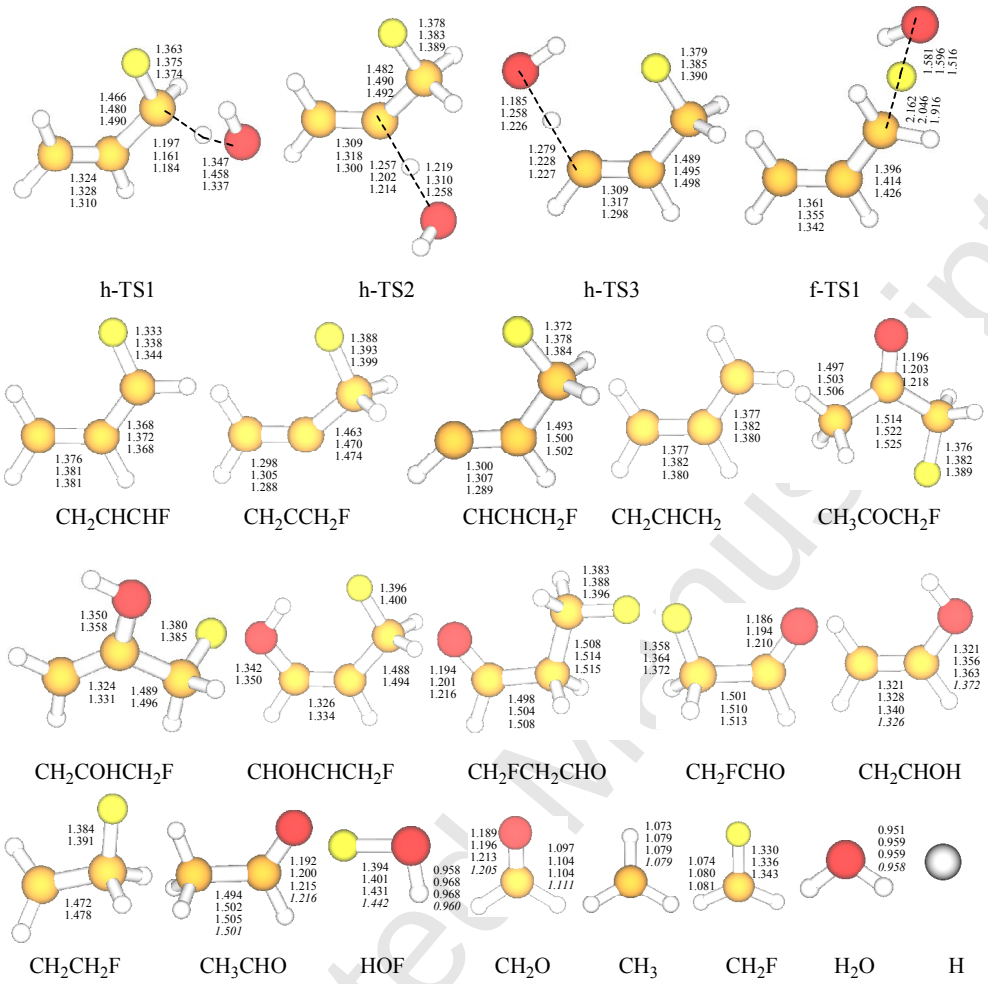

Fig. 1 Optimized geometries (length in Å) of the species of the CH_2=$CHCH_2F$ + OH reaction. The first, second and third entries correspond to the BHandHLYP, M06-2X and MP2 values, respectively. The values in italics are experimental data from ref 30.

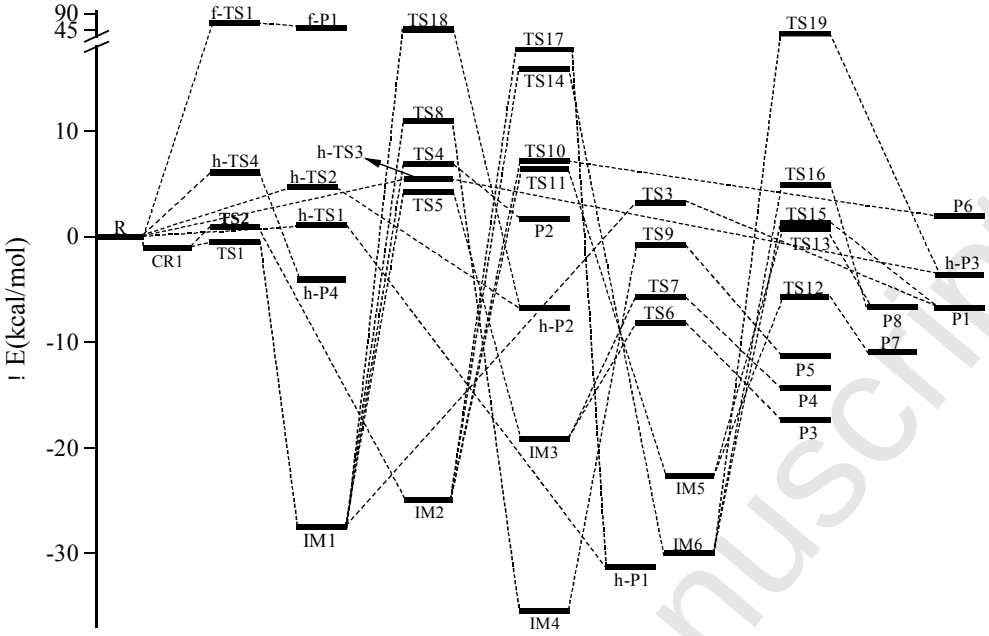

Fig. 2 The profile of potential energy surface for the CH_2=$CHCH_2F$ + OH reaction. The relative energies are calculated at the CCSD(T)/cc-pVTZ//M06-2X/6-311++G(d,p)+ ZPE level of theory.

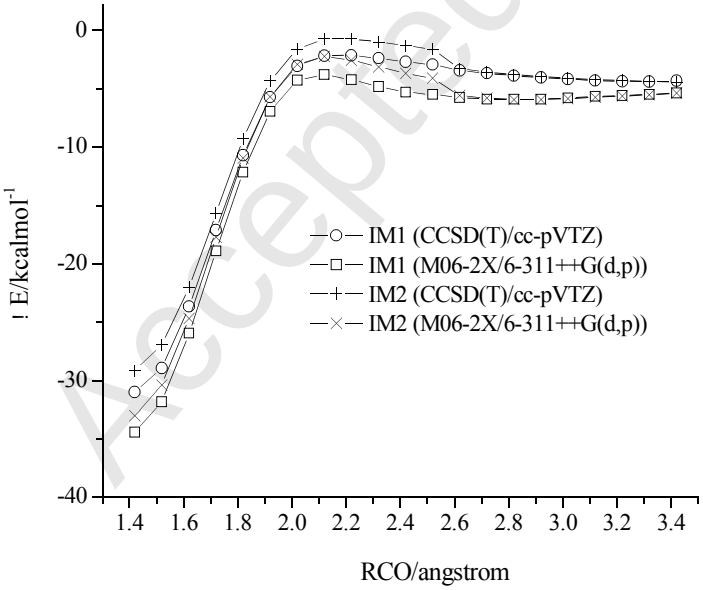

Fig. 3 The calculated minimum energy path along the reaction coordinates (R_{CO}) for the addition of OH to the carbon atoms of CH_2=$CHCH_2F$ at the CCSD(T)/cc-pVTZ and M06-2X/6-311++G(d,p) levels.

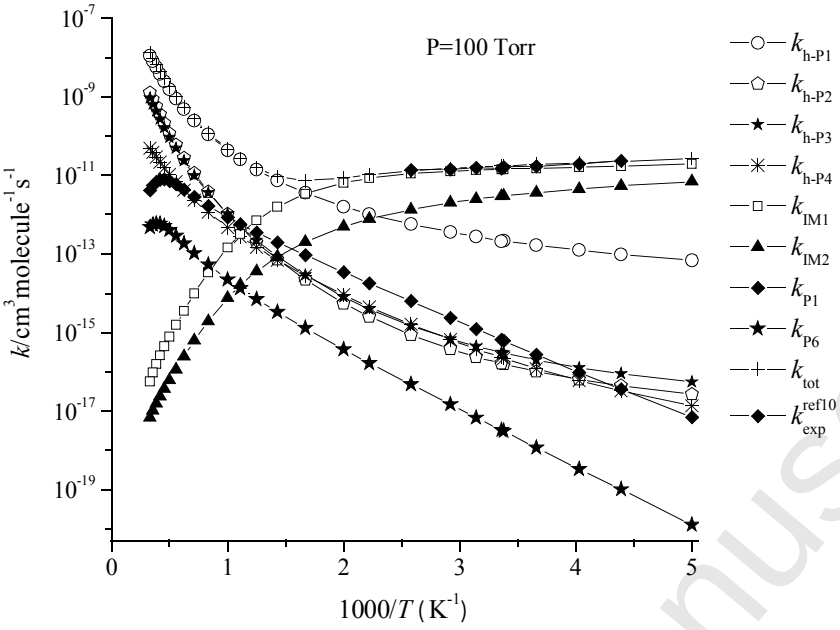

Fig. 4 Temperature dependence of the total and individual rate constants at 100 Torr of He. The experimental data are included from ref 10.

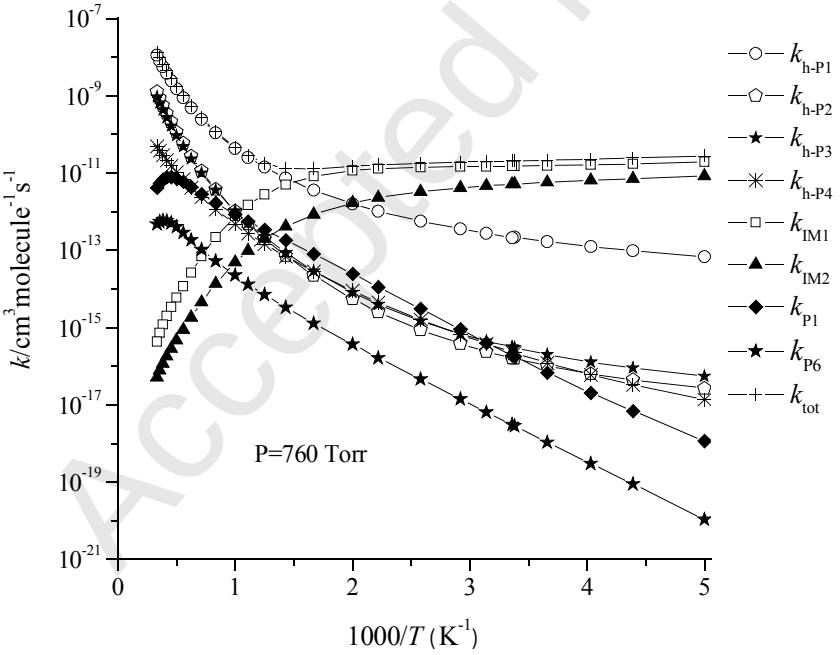

Fig. 5 Temperature dependence of the total and individual rate constants at 760 Torr of He.

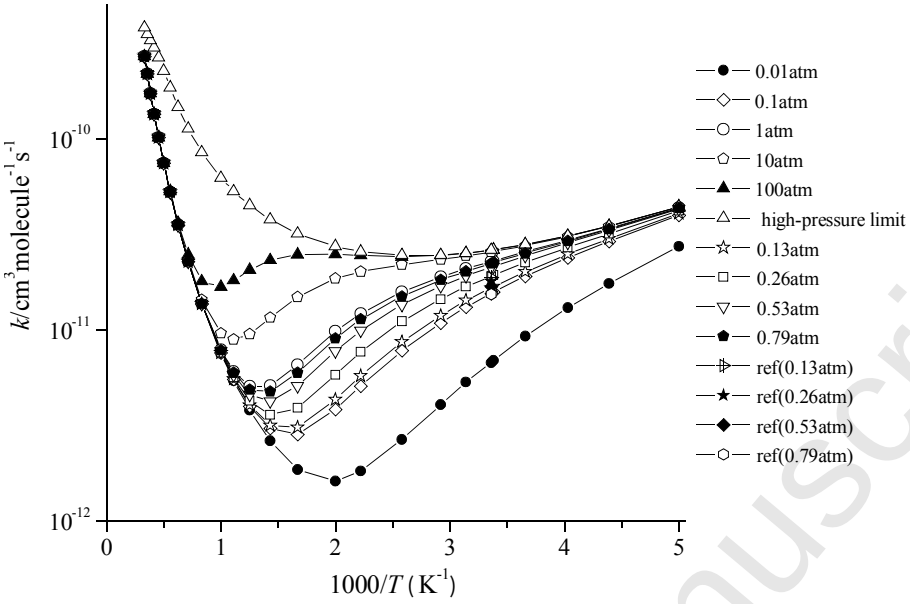

Fig. 6 Total rate constants calculated at several pressures in bath gas of He.

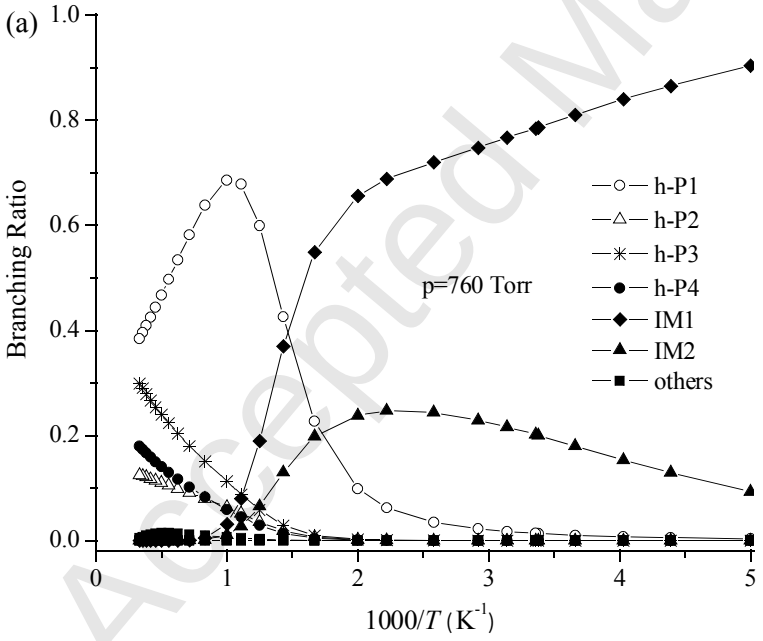

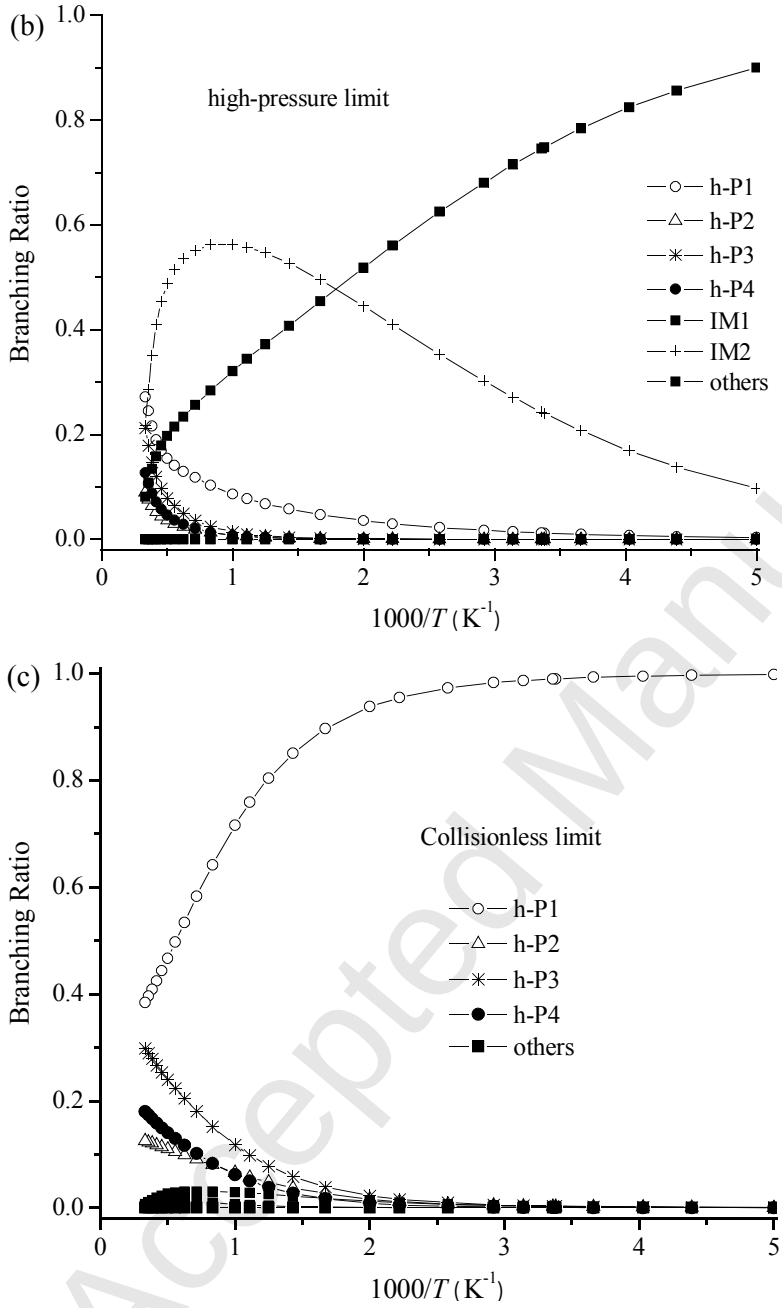

Fig. 7 Branching ratios for the CH_2=$CHCH_2F$ + OH reaction in the temperature range 200-3000 K at (a) atmospheric pressure, (b) high-pressure limit and (c) collisionless limit of He.

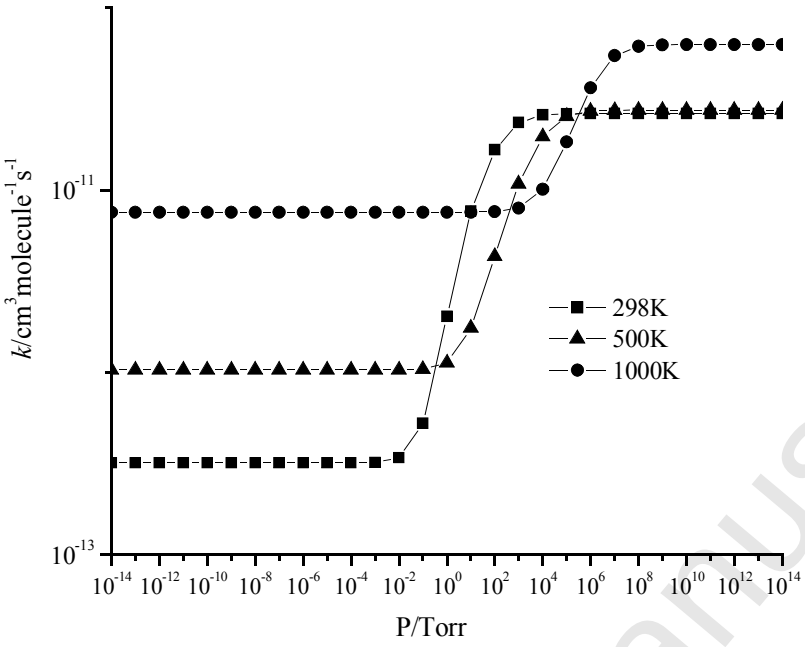

Fig. 8 Pressure dependence of the total rate constants for the CH_2=$CHCH_2F$ + OH reaction at 298, 500 and 1000 K.

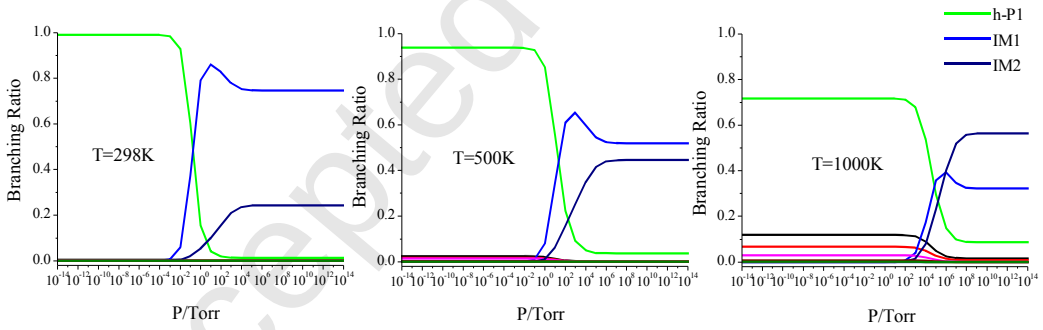

Fig. 9 Branching ratios of products for the CH_2=$CHCH_2F$ + OH reaction at 298, 500 and 1000 K.

Table 1 Relative Energies(! E), T_1 diagnostic values, Reaction Enthalpies(! H) and Gibbs Free Energy(! G) for various species in the OH + CH_2=$CHCH_2F$ reaction

species	T_1[a]	! E[b]	! E[c]	! E[d]	! E[e]	! E[f]	! H[g]	! H[h]	! H[i]	! G[j]
R:CH_2=$CHCH_2F$+OH	0.010 0.007	0.00	0.00	0.00	0.00	0.00	0.00	0.00	0.00	0.00
P1: (CH_2F+CH_2CHOH)	0.014 0.012	-7.86	-6.70	-8.54	-6.65	-6.93	-7.06	-6.74	-6.83	-8.88
P2:(H+CH_2COHCH_2F)	0.012	-0.62	1.66	-0.10	1.83	1.28	1.29	1.81	1.64	4.46
P3:(CH_2F+CH_3CHO)	0.014 0.014	-17.56	-17.39	-17.34	-17.40	-17.20	-17.22	-17.32	-17.31	-19.93
P4:(CH_3+ CH_2FCHO)	0.008 0.013	-14.14	-14.38	-14.08	-14.32	-14.45	-14.19	-14.05	-14.12	-14.99
P5:(H+CH_3COCH_2F)	0.013	-13.25	-11.31	-10.86	-11.40	-11.54	-11.35	-11.19	-11.18	-8.79
P6:(H+$CHOHCHCH_2F$)	0.012	-0.69	1.94	1.16	2.06	2.02	1.94	2.01	1.88	4.58
P7:(CH_2O+CH_2CH_2F)	0.015 0.011	-11.34	-10.96	-10.98	-10.99	-10.95	-10.83	-10.83	-10.83	-13.03
P8:(H+CH_2FCH_2CHO)	0.013	-8.10	-6.66	-6.10	-6.47	-6.66	-8.11	-6.40	-6.56	-4.27
h-P1:(H_2O+CH_2CHCHF)	0.006 0.026	-32.58	-31.57	-35.62	-31.41	-31.27	-30.24	-31.19	-30.92	-32.35
h-P2(H_2O+CH_2CCH_2F)	0.006 0.029	-8.64	-6.58	-11.14	-6.43	-5.20	-4.88	-5.98	-6.33	-7.48
h-P3:(H_2O+cis-$CHCHCH_2F$)	0.006 0.029	-5.45	-3.58	-7.67	-3.46	-2.22	-1.98	-3.12	-3.26	-4.41

h-P4:(H_2O+trans-$CHCHCH_2F$)	0.006 0.029	-6.02	-4.07	-8.23	-4.00	-2.73	-2.51	-3.68	-3.78	-4.88
f-P1:(HOF+CH_2CHCH_2)	0.011 0.028	54.39	49.85	52.20	50.01	49.34	49.23	49.91	49.75	48.22
CR1	0.012	-4.08	-1.60	-2.27	-1.69	-2.08	-2.09	-1.72	-1.79	5.23
IM1	0.012	-30.94	-27.50	-29.03	-27.51	-27.28	-28.30	-28.42	-28.46	-18.91
IM2	0.012	-28.87	-25.01	-26.68	-24.85	-24.66	-25.68	-25.80	-25.98	-16.86
IM3	0.014	-25.92	-19.13	-16.93	-20.52	-22.76	-23.99	-20.76	-20.46	-10.16
IM4	0.014	-39.40	-35.46	-37.57	-35.18	-34.94	-36.02	-36.16	-36.41	-27.08
IM5	0.014	-25.99	-22.70	-20.70	-22.41	-22.04	-23.49	-23.79	-24.08	-13.92
IM6	0.013	-33.18	-29.94	-31.64	-29.72	-29.31	-30.41	-30.64	-30.90	-21.60
TS1	0.028	-1.99	-0.46	-0.31	-0.34	0.78	-0.29	-1.30	-1.42	7.89
TS2	0.028	-0.60	0.94	0.95	1.07	2.00	1.08	0.28	0.05	9.09
TS3	0.024	0.04	3.22	2.33	3.16	3.93	2.95	2.33	2.30	11.66
TS4	0.024	5.53	6.92	6.98	7.60	8.22	6.88	6.40	5.69	15.91
TS5	0.016	2.31	4.29	5.44	4.22	4.82	3.18	2.63	2.70	13.52
TS6	0.024	-10.60	-8.11	-7.63	-8.04	-4.02	-5.19	-9.00	-9.12	0.31
TS7	0.023	-7.90	-5.67	-5.22	-5.82	-4.50	-5.61	-6.72	-6.64	2.81
TS8	0.014	6.56	10.95	7.60	11.12	11.44	10.23	9.95	9.75	19.08
TS9	0.022	-3.55	-0.78	-1.06	-0.46	0.34	-0.66	-1.22	-1.65	7.66
TS10	0.024	4.67	7.20	6.98	7.08	7.68	6.40	5.95	6.08	15.80
TS11	0.017	4.34	6.43	7.52	6.44	7.09	5.50	4.92	4.92	15.27
TS12	0.024	-8.25	-5.73	-5.30	-5.82	-4.54	-5.74	-6.84	-6.81	2.60
TS13	0.022	-1.76	0.77	0.94	0.40	1.31	-0.04	-0.74	-0.42	9.44
TS14	0.015	11.38	15.88	13.33	16.12	16.54	15.36	15.06	14.77	24.32
TS15	0.025	-1.66	1.28	0.54	1.42	2.09	1.26	0.71	0.58	8.72

TS16	0.024	2.48	4.94	5.38	5.27	6.26	5.32	4.36	4.08	13.06
TS17	0.022	23.86	27.86	26.31	—	28.52	26.89	—	26.38	37.07
TS18	0.033	45.99	46.78	45.98	47.79	48.49	47.62	47.13	46.00	55.11
TS19	0.018	35.00	39.14	38.92	39.26	39.01	37.61	37.88	37.71	48.24
h-TS1	0.023	0.34	1.14	0.94	0.64	2.59	1.95	-0.01	0.46	8.74
h-TS2	0.024	3.62	4.76	4.36	4.58	6.95	6.22	3.99	4.10	12.41
h-TS3	0.026	3.42	5.46	5.26	5.88	7.98	7.19	5.10	4.83	13.11
h-TS4	0.025	4.65	6.04	5.67	5.98	8.23	7.56	5.41	5.41	13.82
f-TS1	0.045	63.96	61.96	68.22	59.64	66.38	65.89	59.53	61.68	69.25

The energies are given in kcal/mol. [a]CCSD(T)/cc-pVTZ; [b]M06-2X/6-311++G(d,p); [c]CCSD(T)/cc-pVTZ//M06-2X; [d]MC-QCISD//M06-2X; [e]CCSD(T)/cc-pVTZ//BHandHLYP; [f]CCSD(T)/cc-pVTZ//MP2; [g]CCSD(T)/cc-pVTZ//MP2; [h]CCSD(T)/cc-pVTZ//BHandHLYP; [i]CCSD(T)/cc-pVTZ//M06-2X; [j]CCSD(T)/cc-pVTZ//M06-2X.